

Serendipitous AGN in the *XMM-Newton* fields of Markarian 205 and QSO 0130–403

K.L. Page, M.J.L. Turner, J.N. Reeves, P.T. O’Brien, S. Sembay
X-Ray Astronomy Group, Department of Physics & Astronomy, Leicester, LE1 7RH, UK

Received ** *** 2002 / Accepted ** *** 2002

ABSTRACT

The X-ray spectra of serendipitously observed AGN in the *XMM-Newton* fields of Mrk 205 and QSO 0130–403 are analysed. The sample consists of 23 objects, none of which is detected at radio frequencies, with a median X-ray luminosity of $\sim 4 \times 10^{44}$ erg s $^{-1}$ and redshifts ranging from ~ 0.1 to just over 3. The mean photon index was found to be 1.89 ± 0.04 . In contrast to past *ASCA* and *ROSAT* observations of high-redshift radio-loud quasars, we find little evidence for excess intrinsic absorption in these radio-quiet objects, with only three sources requiring a column density in excess of the Galactic value. Comparing the measured spectral indices over the redshift range, we also find there is no X-ray spectral evolution of QSOs with time, up to redshift 3. Within the sample there is no evidence for evolution of the optical to X-ray spectral index, α_{ox} , with redshift, the mean value being -1.66 ± 0.04 . However, upon comparing the values from the Bright Quasar Survey at low redshift ($z < 0.5$) and high redshift QSOs detected by Chandra ($z > 4$), a slight steepening of α_{ox} is noted for the more distant objects. In most of the sources there is no significant requirement for a soft excess, although a weak thermal component (≤ 10 per cent of L_X) cannot be excluded. There is an indication of spectral flattening (by $\Delta\Gamma = 0.2$) at higher energies (> 3 keV, QSO rest frame) for the sample as a whole. This is consistent with the presence of a Compton reflection component in these radio-quiet AGN, with the scattering medium (such as an accretion disc or molecular torus) occupying a solid angle of 2π steradians to the X-ray source.

Key words: galaxies: active – X-rays: galaxies – quasars: general

1 INTRODUCTION

The majority of luminous AGN (Active Galactic Nuclei) are found to be radio-quiet (e.g., Kukula *et al.* 1998); that is, the radio (5 GHz) to optical (*B*-band) flux ratio is ≤ 10 (Wilkes & Elvis 1987; Kellerman *et al.* 1989). The radio emission of radio-quiet QSOs is not non-existent, but is about 100 times less than that of the radio-loud quasars. In general, for a given optical luminosity, the average X-ray emission from radio-quiet AGN is about three times lower than that from radio-loud objects (Zamorani *et al.* 1981; Worrall *et al.* 1987). For this reason, they are more difficult to detect at higher redshifts, so the majority of distant AGN studied so far in the X-ray band are radio-loud. One method of increasing the number of high-*z* radio-quiet objects observed is to make use of the field sources in deep observations taken with a sensitive instrument, such as *XMM-Newton*. In this paper we present a study of the background field sources from two long *XMM-Newton* observations; for both fields optical identifications exist, so that the redshift and optical classification of each object are known.

Although unified models exist, claiming that most AGN subclasses can be understood simply through orientation effects (see Antonucci 1993 and references therein), the difference between radio-quiet and radio-loud QSOs (RQQs and RLQs) has yet to be completely explained.

It was once thought that RQQs were only found in spiral galaxies, while the RLQs inhabited ellipticals. However, advances in observing capability now show that as many as 50 per cent of the RQQs discovered may occur in ellipticals (e.g., Véron-Cetty & Woltjer 1990). RLQs, however, are almost exclusively found in bulge-dominated systems; that is, in ellipticals or early-type spirals (Falomo, Kotilainen & Treves 2001).

The *Einstein* IPC (Imaging Proportional Counter) data showed that radio-quiet and radio-loud objects have different power law slopes over the energy range 0.4–4 keV, with the RQQs being steeper (e.g., Wilkes & Elvis 1987). Follow-up with *ROSAT* (Brinkmann, Yuan & Siebert 1997; Yuan *et al.* 1998) confirmed these findings for the soft X-ray band and *Ginga* (Williams *et al.* 1992), *EXOSAT* (Lawson *et al.* 1992) and *ASCA* (Reeves *et al.* 1997; Reeves & Turner 2000

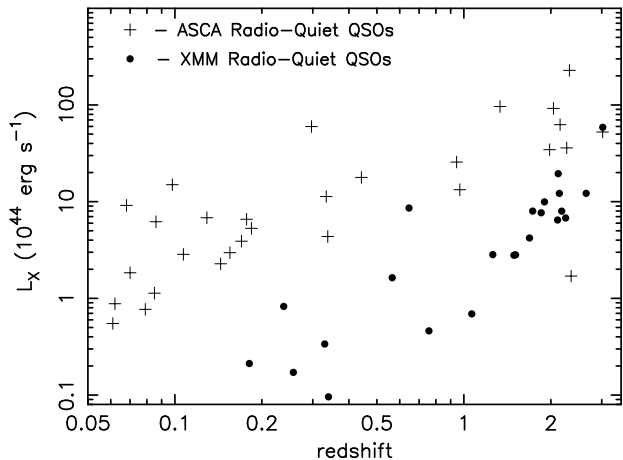


Figure 1. The luminosities of radio-quiet objects are plotted against redshift. Measurements marked as crosses are taken from Reeves & Turner (2000); circles are from this paper.

– RT00 hereafter) for the harder X-ray energies. This observed difference in slope ($\Delta\Gamma \sim 0.3$ over 2–10 keV – Lawson *et al.* 1992; $\Delta\Gamma \sim 0.5$ in the 0.2–3.5 keV band – Wilkes & Elvis 1987) may be due to an extra, hard X-ray component linked to the radio emission of RLQs; i.e., connected with the radio-jets.

Neither *Einstein* (Canizares & White 1989; Wilkes & Elvis 1987) nor *ROSAT* (Yuan *et al.* 1998) found any indication for excess absorption in radio-quiet QSOs. Yuan *et al.* (1998) also found that the mean spectral slope of nearby RQQs is consistent with that of more distant ($z > 2.5$) QSOs, implying that X-ray spectral evolution may be unimportant in the radio-quiet objects.

Because of the effective area of its mirrors, *XMM-Newton* can obtain spectra of fainter objects for a given redshift than could any previous X-ray instrument. This allows us to extend previous surveys of QSOs to include those objects with lower luminosity and to observe a given luminosity at a wider range of redshifts. In this respect, the luminosities of the objects presented in this paper (median value of $\sim 4 \times 10^{44}$ erg s $^{-1}$) are closer to those of the AGN which make up the cosmic X-ray background. Fig. 1 shows the luminosity distribution of radio-quiet objects surveyed by *XMM* in this paper compared, with those surveyed by *ASCA* in RT00.

In Section 2 the data reduction is discussed, with the spectral fitting to the individual objects outlined in Section 3. The highest-flux objects are analysed in 4, while the work on Mrk 205 itself was presented in a separate paper (Reeves *et al.* 2001). Finally, the results are discussed in Section 5.

2 XMM-NEWTON OBSERVATIONS

The objects in this paper were serendipitously located in the fields of two *XMM* pointed observations: Mrk 205 and QSO 0130–403. The Mrk 205 data are from a calibration observation, in May 2000 (OBS ID 0124110101). There were three separate exposures with both the MOS and PN cameras (Turner *et al.* 2001; Strüder *et al.* 2001), each of which

lasted for ~ 17 ksec, and these were co-added before spectral analysis was performed. QSO 0130–403 was observed only once, for ~ 37 ksec, in June 2001 (OBS ID0112630201).

The optical identifications and redshifts for the Mrk 205 field are taken from Barcons *et al.* (2002), henceforth XB02, which also quotes X-ray colours and fluxes. For the QSO 0130–403 field, the IDs were taken from the Véron-Véron 2001 catalogue. Hence, the Mrk 205 objects were selected on the basis of their X-ray flux ($> 2 \times 10^{14}$ erg cm $^{-2}$ s $^{-1}$ in the 0.5–4.5 keV band; XB02), with all objects down to this flux level and not in a CCD chip-gap included. The objects analysed in the second field were those which had existing optical identifications; all the optically-selected QSOs within the *XMM* field of view were detected and included in the sample.

In general, one might expect that X-ray-selected targets would show harder spectra than those found through optical observations, simply because soft X-ray sources are not as easy to detect, due to Galactic absorption. Comparing both the slopes over 2–10 (rest frame) and 0.2–10 (observed frame) keV for the objects in the two separate fields, a mean difference of $\Delta\Gamma < 0.1$ is found. The actual range of photon indices is also very similar for both of the fields, with the vast majority (~ 80 per cent) of the spectral slopes lying between $\Gamma \sim 1.6$ –2.4. The similarity in the distributions of indices implies that there is no obvious problem in combining these two fields.

The data obtained allow individual spectral fitting for the QSOs in these fields. We present these spectra and investigate the sample as a whole, to determine whether there is any evidence for evolution, Compton reflection or excess absorption in the rest frames of the objects. A wide range of redshifts, from $z = 0.181$ to 3.023, is covered.

The data were reduced with the *XMM* SAS (Science Analysis Software) version 5.2, using EPCHAIN and EMCHAIN to generate valid photon lists; further filtering was then performed using XMMSELECT. Both single and double pixel events (patterns 0–4) were used when extracting the PN spectra, while patterns 0–12 were chosen for the MOS exposures. Each spectrum was extracted using a circular region of 30 arcsec radius, with the same circle then offset from the source to obtain an estimate of the background.

Since the sources were not all close to the centre of the CCDs, ARFGEN was run within the SAS, to correct for vignetting effects and the encircled energy fraction. Subsequently, CCD redistribution matrices (i.e., *.rmf* not *.rsp*) were used. The energy resolution of the PN chips changes as one moves out from the centre, due to charge transfer effects; to take this into account, PN rmfs are provided at intervals of 20 rows, with Y0 being used for rows 1–20 (furthest from the centre) up to Y9 for the central objects. For example, epn_ff20_sdY9_qe.rmf was used with ARFGEN for a central source (Y9), extracted for patterns 0–4 (sd = singles and doubles) in a full-frame (ff) image. Note that, for pure redistribution matrices, the type of filter (thin, medium or thick) is not included; this becomes part of the ancillary response function (arf) generated. For MOS, the relevant responses were m1_r5_all_15.rmf and m2_r5_all_15.rmf (all meaning the spectra were extracted for patterns 0–12). See <http://xmm.vilspa.esa.es/ccf/epic> for more details.

After using the FTOOL command GRPPHA, to provide a minimum of 20 counts per bin, the XSPEC v11.0.1 software

package was used to analyse the background-subtracted spectra. The value of the Galactic absorption was obtained using the `FTOOL` N_H , which uses data from Dickey & Lockman (1990). N_H was found to be $3 \times 10^{20} \text{ cm}^{-2}$ for the Mrk 205 field and $1.9 \times 10^{20} \text{ cm}^{-2}$ for the QSO 0130–403 field. H_0 was taken to be $50 \text{ km s}^{-1} \text{ Mpc}^{-1}$ and q_0 to be 0.5. Unless stated otherwise, the errors given are at the 1σ level.

Of the 23 AGN analysed in this paper, only two (XMMU J013257.8-401030 and XMMU J013333.8-395554) have actual (upper limit) radio observations, of 0.4 mJy at 5 GHz (Miller, Peacock & Mead 1990). None of the others are detected in the NVSS (NRAO VLA Sky Survey), down to the survey completeness flux limit of about 2.5 mJy. Using this flux limit (and the two actual upper limits), we find that six of the AGN are definitely radio-quiet. Although the remaining seventeen objects could be radio-loud, it is found that (again using the NVSS survey limit) most would only be slightly so, with twelve having $R < 60$.

Statistically, one would expect ~ 20 per cent of the BLAGN (with X-ray fluxes above $10^{-14} \text{ erg cm}^{-2} \text{ s}^{-1}$) in an XMM field to be radio loud (based on studies of sources within the XMM observation of the Lockman Hole; private communication, Lehmann 2002); this corresponds to ~ 4 objects in a sample of this size. However, as our survey does not go as deep as $10^{-14} \text{ erg cm}^{-2} \text{ s}^{-1}$, it should be expected that this is an upper limit to the number of radio-loud sources.

3 SPECTRAL ANALYSIS

As is conventional, the spectrum for each source was first modelled using a simple power law, together with neutral hydrogen absorption fixed at the Galactic value. The majority of sources were seen with both the MOS and PN, although the occasional source would be positioned in one of the chip gaps, or over a bad column. Where both MOS and PN CCDs could be used, joint fits were performed. For sixteen of the QSOs, the single power law model produced a good fit, with $\chi^2_\nu \sim 0.8$ –1.2. The remaining seven objects showed slightly worse statistics, but the fits were still acceptable.

Table 1 lists the redshift and optical magnitude (from XB02 for the Mrk 205 field and NED – the NASA Extragalactic Database – for the objects around QSO 0130–403), count-rate, flux, luminosity and 2–10 keV (QSO rest frame) spectral slope (all derived from our data) for each of the 23 sources. All but three of the objects in this sample are Broad Line AGN (BLAGN). XMMU J122120.5+751616 and XMMU J122206.4+752613 are classified as Narrow Emission Line AGN (NLAGN) by XB02, with XMMU J122258.1+751934 tentatively classified as the same. It should be noted that the optical spectrum for this last object is not of high quality and there is, therefore, some uncertainty in the given redshift of 0.257. It can be seen from the column giving the luminosities that all except two of the objects have a 2–10 keV luminosity of $> 10^{43} \text{ erg s}^{-1}$; they should, therefore, be classified as QSOs, rather than any of the lower-luminosity objects which come under the title of AGN.

Over the 2–10 keV (rest-frame) band, the weighted mean of the photon index for all 23 objects was found to be

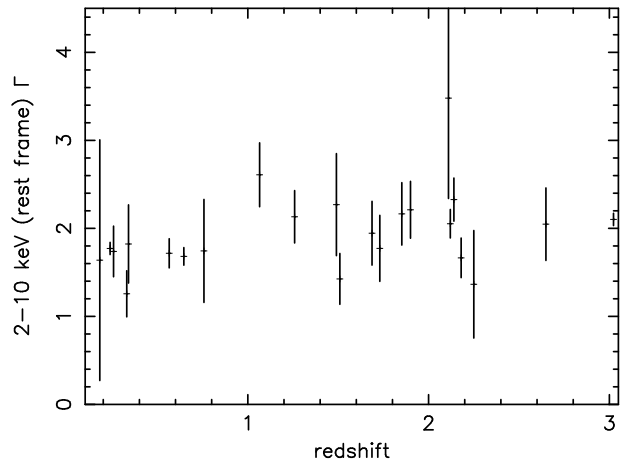


Figure 2. Plot of 2–10 keV Γ against redshift for each of the 23 sources. No clear trend between Γ and z is found for the sample.

$\Gamma = 1.89 \pm 0.04$. The dispersion of the slopes from the mean, taking into account the measurement errors, is $\sigma \sim 0.21$ (see Fig 2). Using the more rigorous Maximum Likelihood method (Maccacaro *et al.* 1988), the dispersion was calculated to be 0.29 ± 0.04 . The mean of the 2–10 keV photon index for the RLQs in RT00 is given as 1.66 ± 0.04 , while the RQQs had a mean Γ of 1.89 ± 0.05 . It can be seen that the XMM-observed radio quiet objects in this paper have a mean slope which is in excellent agreement with the higher flux objects measured by *ASCA* and that the radio-loud *ASCA* objects have a flatter index ($\Delta\Gamma \sim 0.2$), corroborating the known difference between radio-loud and radio-quiet QSOs found in previous surveys.

3.1 Soft Excess and Absorbing Column Density

For each source, a low-energy blackbody component was added, to see if there was a measurable soft excess; however, it was found that, statistically, only one of the sources required this addition: XMMU J122135.5+750914 was better fitted by the inclusion of a blackbody component with $kT = 0.152 \pm 0.031 \text{ keV}$. The luminosity of the soft excess component was ~ 18 per cent that of the power law.

Excess absorption in the QSO rest frame was also investigated, using the *zwabs* model in XSPEC to include a component in addition to the Galactic column density. Only three of the sources in the joint fields showed any improvement in the reduced χ^2 , one of which (XMMU J122344.7+751922) then gained an extremely steep ($\Gamma \sim 3.5$) spectral slope, for an excess absorption of $(2.27 \pm 1.06) \times 10^{21} \text{ cm}^{-2}$. The other two objects, both classed as NLAGN, were XMMU J122206.4+752613, with an improvement in χ^2 of 40, for one degree of freedom, for an additional column density of $(6.0 \pm 1.0) \times 10^{20} \text{ cm}^{-2}$ and XMMU J122258.1+751934, showing a decrease in χ^2 of six for one degree of freedom, for $N_H = (1.28 \pm 0.64) \times 10^{21} \text{ cm}^{-2}$. All three of these objects are of low luminosity.

Although the higher redshift objects appeared to show larger upper limits for the absorbing column density, it should be noted that this is likely to be related to the shift in energy bandpass. For an object with $z = 3$, the 0.2–10 keV

Table 1. QSOs with known redshifts in the fields of Mrk 205 and QSO 0130–403. The luminosity was calculated for $q_0 = 0.5$ and $H_0 = 50 \text{ km s}^{-1} \text{ Mpc}^{-1}$; the absorption-corrected value is given for the QSO rest-frame 2–10 keV band. The optical magnitudes given are g' for the Mrk 205 field objects and V-band for QSO 0130–403. Alternative names for the QSOs in the QSO 0130–403 field are given at the foot of the table. VV01 indicates the Véron-Véron catalogue (Véron-Cetty & Véron 2001)

Source ID	z	0.2–10 keV Count Rate ¹ (10^{-3} s^{-1})	2–10 keV Flux (10^{-14} $\text{erg cm}^{-2} \text{ s}^{-1}$)	2–10 keV Luminosity ($10^{44} \text{ erg s}^{-1}$)	Optical Magnitude	2–10 keV rest frame Γ
XMMU J121819.4+751919	2.649	7.39 ± 1.10	1.49	38.20	19.79	2.05 ± 0.41
XMMU J122048.4+751804	1.687	13.01 ± 1.19	3.13	4.25	18.97	1.95 ± 0.36
XMMU J122051.7+752820	0.181	2.95 ± 1.11	1.32	0.022	22.05	1.64 ± 1.37
XMMU J122052.0+750529	0.646	65.75 ± 1.91	41.97	8.63	18.62	1.68 ± 0.10
XMMU J122111.2+751117	1.259	17.83 ± 1.17	2.56	2.87	19.54	2.13 ± 0.30
XMMU J122120.5+751616	0.340	16.28 ± 1.23	1.60	0.096	20.90	1.82 ± 0.44
XMMU J122135.5+750914	0.330	13.78 ± 1.15	5.85	0.29	20.38	1.26 ± 0.26
XMMU J122206.4+752613	0.238	115.2 ± 1.89	36.85	0.91	20.03	1.77 ± 0.77
XMMU J122242.6+751434	1.065	6.05 ± 1.14	0.35	0.28	21.82	2.61 ± 0.36
XMMU J122258.1+751934	0.257	12.86 ± 1.20	7.07	0.20	22.66	1.74 ± 0.29
XMMU J122318.5+751504	1.509	7.72 ± 1.13	1.70	3.00	21.15	1.43 ± 0.29
XMMU J122344.7+751922	0.757	9.87 ± 1.26	1.01	0.46	20.69	1.77 ± 0.59
XMMU J122351.0+752227	0.565	33.81 ± 1.71	10.17	1.63	19.93	1.72 ± 0.17
XMMU J122445.5+752224	1.852	9.68 ± 1.40	3.80	7.67	20.16	2.17 ± 0.36
XMMU J013302.0–400628 ^a	3.023	74.44 ± 1.89	7.63	82.80	17.4	2.10 ± 0.07
XMMU J013257.8–401030 ^b	2.180	17.96 ± 1.42	2.74	7.46	19.2	1.67 ± 0.23
XMMU J013314.7–401212 ^c	1.49	4.82 ± 0.43	1.09	2.82	19.0	2.27 ± 0.58
XMMU J013205.4–400047 ^d	2.12	25.82 ± 1.46	4.57	18.60	20.16	2.05 ± 0.16
XMMU J013348.3–400233 ^e	2.11	2.49 ± 0.37	3.68	5.87	20.3	3.48 ± 1.14
XMMU J013233.2–395445 ^f	1.73	3.14 ± 0.37	5.37	7.49	20.3	1.77 ± 0.38
XMMU J013333.8–395554 ^g	1.90	3.98 ± 0.41	3.52	9.41	19.8	2.21 ± 0.32
XMMU J013408.6–400547 ^h	2.14	17.06 ± 0.13	1.90	12.30	19.56	2.33 ± 0.25
XMMU J013320.4–402021 ⁱ	2.25	4.37 ± 1.06	3.87	6.98	20.5	1.37 ± 0.61

¹ PN count rate, unless MOS data only available.

^a QSO 0130–403; ^b [VV01] J013257.5–401028; ^c [VV01] J013315.2–401203; ^d [VV01] 013205.4–400048; ^e [VV01] J013348.2–400235;

^f [VV01] J013233.2–395445; ^g [VV01] 013334.1–395546; ^h [VV01] 013408.5–400547; ⁱ [VV01] J013320.4–402022

observed band corresponds to 0.8–40 keV in its rest frame. It is, therefore, obvious that there will be increased difficulty in measuring moderately small absorption related to the softest X-ray photons and, so, a higher upper limit will be found compared to a source of the same flux at a lower redshift.

We also tried fixing the photon index to a typical value of $\Gamma = 1.9$ (e.g., Nandra & Pounds 1994), to see whether the apparent dispersion in Γ could be explained by excess absorption in the QSO rest frame; i.e., to see if any of the flat spectral slopes were due to the objects being obscured. The model comprised a direct, absorbed power law, together with a scattered, unabsorbed component (both with $\Gamma = 1.9$). However, for ten of the objects in the sample, this produced a worse fit than that with no obscuration component and only four sources were significantly better-fitted using this model – the two NLAGN which required the *zwabs* column density, together with XMMU J122052.0+750529 and XMMU J122135.5+750914. The obscuring columns found for the NLAGN were (2.40 ± 0.57) and $(1.75 \pm 1.57) \times 10^{21} \text{ cm}^{-2}$, while the BLAGN objects required (7.73 ± 4.88) and $(17.88 \pm 11.85) \times 10^{22} \text{ cm}^{-2}$ respectively. The remaining nine objects can be equally well fitted by either a simple power law, or by including the obscured component. It should be noted that the objects with particularly flat spectral indices are all included in this group.

Although, statistically, these nine spectra can be fitted by the inclusion of an obscuring column density, the values for N_H are not well constrained and are entirely consistent with zero. This implies that the more complicated model is not required and that these QSO nuclei are not heavily absorbed, consistent with AGN unification schemes where one should observe a direct line to the nucleus in these type-1 AGN. To summarise, there appears to be an intrinsic dispersion in the primary X-ray power law slopes of these background AGN, which cannot be solely caused by line of sight absorption.

In order to try and obtain better statistics for the fits, it was decided to co-add spectra over three redshift ranges – $z = 0-1$, $1-2$ and > 2 – and look at the subsequent continuum shapes. For each grouping, an average background spectrum was produced and the mean redshift calculated. Although co-adding spectra will tend to blur sharp features, such as iron emission lines, this should not be a problem when simply looking at the continuum as a whole.

Only the resulting spectrum for the low-redshift group (mean $z = 0.4$) required excess absorption, with an additional column density of $(2.9 \pm 0.9) \times 10^{20} \text{ cm}^{-2}$ for $\Gamma = 1.83 \pm 0.03$. Such a column would be undetectable at higher redshifts, as it would be shifted out of the *XMM-Newton* bandpass. Even with the better statistics derived from the co-adding of the spectra, there was still no requirement for a blackbody component for either the low-

or medium-redshift group, with the luminosity of the soft component being <6 per cent of the total X-ray luminosity. For the highest-redshift objects, however, a blackbody does improve the fit significantly: a temperature of $kT = 0.214 \pm 0.043$ leads to a reduction in χ^2 of 8, for 2 degrees of freedom (>90 per cent confidence, using the F-test), with the luminosity of the BB component being almost 15 per cent that of the power law. However, as is discussed in Section 3.3, some of this spectral curvature could be due to reflection.

As an alternative method for identifying curvature due to a soft excess, the lowest-redshift co-added spectrum was fitted with a broken power law, with the break at 2 keV in the rest frame. Γ was measured to be 1.86 ± 0.10 below the break and 1.82 ± 0.05 above. Hence, there is little steepening of the spectrum at lower energies, the upper limit being $\Delta\Gamma < 0.18$; this is consistent with the finding above, that any soft excess present in the low redshift objects is only weak.

3.2 Spectral Evolution

Fig. 2 shows the 2–10 keV power law indices versus redshift. The dispersion in Γ is clearly visible, but there is no noticeable trend with z . A basic Spearman-Rank test to the broad-band photon index versus redshift data implied there was no correlation between the values.

Weighted linear regression was then performed, producing a best-fit slope to the Γ - z graph of 0.14 ± 0.03 . However, five measurements have rather small errors and so may be biasing the result; these were, therefore, removed and the statistic recalculated. This gave a value for the gradient of 0.07 ± 0.12 , so implying that there is little, or no, correlation between the spectral slope and the redshift for the objects analysed. This lack of correlation is also noted for the Γ -luminosity data, as would be expected from the tight correlation between L_X and redshift.

Values of the two-point optical to X-ray spectral index, α_{ox} , were measured, where

$$\alpha_{ox} = \frac{\log \frac{f_{\nu}(2keV)}{f_{\nu}(2500A)}}{\log \frac{\nu(2keV)}{\nu(2500A)}}$$

and the mean calculated to be -1.66 ± 0.04 . For this sample alone, no correlation was found between α_{ox} and redshift. However, previous results from the Bright Quasar Survey (BQS) gave a slightly flatter value of $\alpha_{ox} = -1.56 \pm 0.02$, for unabsorbed QSOs at low redshift (with $z < 0.5$), while the mean slope found by Chandra for the more distant ($z > 4$) objects is somewhat steeper, at -1.78 ± 0.03 (both values from Vignali *et al.* 2001). Comparing these measurements from the BQS, Chandra and XMM, there is an indication that α_{ox} steepens slightly with increasing redshift, with the extreme high redshift QSOs (at $z > 4$) being relatively fainter in the X-ray band, compared to low- z objects. One should be cautious when comparing samples of optically-selected (e.g., BQS) and X-ray-selected objects, since selection biases may lead to complications. However, some studies (e.g., Lamer, Brunner & Staubert 1997) have shown that the differences are not always significant. Likewise, as mentioned in Section 2, the differently-selected fields in this paper show a consistent range of spectral parameters.

3.3 Spectral Curvature

AGN, as a group, often show ‘reflection’ features, due to back-irradiation of the accretion disc by the hard X-ray flux (Pounds *et al.* 1990; Nandra & Pounds 1994), the strength of the features depending on the solid angle subtended by the optically thick, reflecting material. The strongest of these features is often an emission line arising from iron fluorescence, at ~ 6.4 – 6.9 keV, depending on the ionisation state of the material. An absorption edge, located at 7.1 keV (for neutral iron), should also be visible. The individual spectra we obtained show no obvious features around this energy range, possibly because of limited signal-to-noise. The ‘Compton reflection hump’ (which flattens the high energy spectrum) occurs due to the decreasing photo-electric absorption opacity and is expected to peak around 20–40 keV in the rest frame of the object. Because of the high redshift of the objects in this sample, the observed XMM energy band extends to up to 30–40 keV in the rest frame and, so, the spectra might be expected to show evidence of the Compton hump.

Neutral reflection models were tried (*pearrv* in XSPEC; Magdziarz & Zdziarski 1995), fixing the exponential energy cut-off at 100 keV and the disc inclination angle at 30° . The strength of the reflection component is given by $R = \Omega/2\pi$, where Ω is the solid angle subtended by the reflector. Upon fitting the AGN individually, only one of the brightest objects, QSO 0130–403, showed evidence for reflection, with χ^2 decreasing by 16 for 1 degree of freedom, corresponding to a probability of >99.99 per cent via an F-test.

A simpler method, more appropriate to the limited data quality, was to try and identify spectral curvature by measuring the photon index over two distinct energy bands (defined as 0.5–3 keV and 3+ keV in the rest frame of the object) and hence determine the difference between the ‘hard’ and ‘soft’-band values. The values of the slope in all energy bands analysed are shown in Table 2. At the foot of each column, the mean value for the photon index in that energy range is given.

If Compton reflection is present, then one would expect the higher-energy spectral slope to be flatter, hence subtracting the soft-band Γ from the harder one would lead to a negative value. Simulations were performed, for an object at the mean redshift of our sample ($z = 1.4$), setting $R = 1$ (corresponding to reflection from the full 2π steradians of Compton thick matter); Γ was then measured over the two energy bands defined above (0.5–3 keV and 3+ keV) and the difference in photon index over the two bands was calculated to be $\Delta\Gamma \sim -0.17$. The weighted mean for the difference in the slopes for our actual spectra was found to be -0.15 ± 0.06 , which corresponds to a reflection component, R , of 0.88 ± 0.35 . The spectral shape for the sample as a whole is therefore consistent with reflection from approximately 2π steradians of optically thick matter, located out of the direct line of sight (such as an accretion disc or molecular torus).

As when investigating the presence of a soft excess and additional absorption, the coadded spectra over three redshift bands were analysed. The photon indices were measured over 0.5–3 keV (rest frame) and 3+ keV energy bands, to compare with the findings above. For the lowest-redshift objects, there was no noticeable change in slope; however,

flattening at the higher-energies of $\Delta\Gamma = -0.25 \pm 0.18$ and -0.30 ± 0.09 were calculated for the middle- and high-redshift groups respectively. This prompted the use of *pearrav*, which indicated the presence of a reflection component (detected at 98 per cent significance), of $R \gtrsim 0.9$ for the most distant objects; there was little improvement in the fit for the medium- z group. This is consistent with the result obtained from finding the average change in slope between the soft and hard energy bands for the individual spectra.

In Section 3.1, the possibility of a soft excess was discussed. Adding in a blackbody component to the model for the high- z group gave an acceptable fit, although, statistically, not as good as for reflection. It also seems unlikely that there would be a more clearly detectable soft excess at higher redshifts than the lower- z values, which are more sensitive to any excess at the lowest energies. Nonetheless, a model comprising both a blackbody and a reflection component still improved the fit, giving a $\chi^2_\nu = 142/144$, corresponding to almost 97 per cent confidence for the addition of the reflection component. Thus, there does appear to be an indication of the Compton reflection hump, in the most distant objects.

4 HIGH FLUX OBJECTS

Within this sample of AGN are 7 objects with 2–10 keV fluxes of greater than 5×10^{-14} erg cm $^{-2}$ s $^{-1}$. These have spectra with sufficiently good signal-to-noise to allow individual analysis in greater detail.

The central object of the second field, QSO 0130–403 (XMMU J013302.0-400628 in the tables), has the highest *luminosity*, at 8.28×10^{45} erg s $^{-1}$. The QSO was discovered by Smith (1976) on Tololo survey plates and found to be a very blue object, from the optical photometry published by Adam (1985). It has previously been observed in the low-energy X-ray region by the *ROSAT* PSPC (Position Sensitive Proportional Counter), which gave a value of $\Gamma = 1.69^{+0.71}_{-0.60}$, when fixing N_H to the Galactic value (Bechtold *et al.* 1994).

When fitting the 2–10 keV rest-frame band, the addition of an ionised Fe emission line, with the line width (σ) set to 0.1 keV, decreased χ^2 by 5 for 2 degrees of freedom, which corresponds to a marginal detection at >90 per cent. (The width of the line could not be well constrained: $\sigma = 0.34 \pm 0.29$). Over the full 0.2–10 keV observed band (corresponding to 0.8–40.2 keV rest frame), the best fit model consists simply of a power law ($\Gamma = 2.09 \pm 0.03$) and the emission line, detailed above, at 6.62 ± 0.12 keV, the equivalent width of the line being ~ 200 eV in the QSO rest frame (~ 50 eV observed). There is no requirement for additional column density or a soft excess. The spectrum is shown in Figure 3.

As mentioned in section 3.3, there is evidence for neutral reflection in this spectrum, with the 90 per cent confidence range for R being 1.11–3.85; i.e. consistent with reflection from the full 2π steradians of an accretion disc.

As stated earlier, most of the spectra did not require the presence of a strong soft excess. For each of the high flux objects, a blackbody component was added into the model, with the temperature fixed at 0.1 keV; the 90 per cent upper limit was then calculated for the luminosity over 0.2–10 keV;

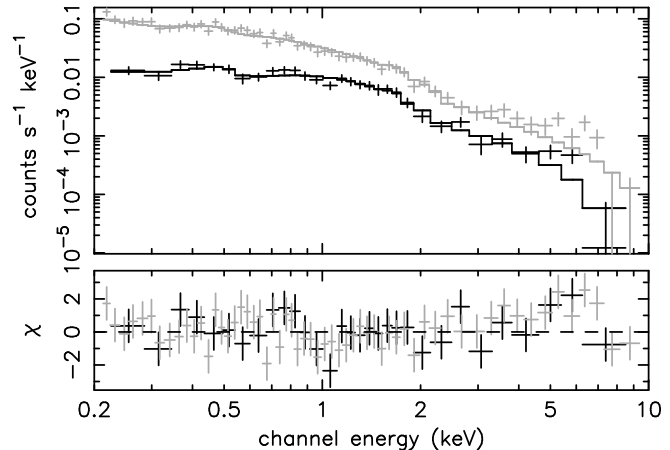


Figure 3. The broad-band spectrum of QSO 0130–403 is best fitted by a power law of $\Gamma \sim 2.09$ and a broad Fe emission line at 6.6 keV (rest frame energy). The MOS spectrum is shown in black and the PN in grey.

in general this was found to be ≤ 10 per cent of the strength of the power law. For a low-luminosity QSO, such as Mrk 205 (Reeves *et al.* 2001), this is a typical value for the relative strength of the soft excess compared to the power law component; thus, the objects in this sample are consistent with other low-luminosity QSOs, where better signal-to-noise in the spectra allow more detailed analysis of the soft excesses.

All the high-flux spectra (Figure 4) were systematically fitted to search for the presence of iron lines and reflection. With the exception of QSO 0130–403, neither iron emission nor the Compton Reflection Hump could be constrained in any of the individual spectra, with 90 per cent upper limits on the equivalent widths of the iron lines lying between 145–650 eV.

It should be noted that two of these bright objects are those classified as Narrow Line AGN by XB02 – XMMU J122206.4+752613 and XMMU J122258.1+751934. These are the only two high-flux objects which have measurable excess absorption; the values, however ($\leq \text{few} \times 10^{21}$ cm $^{-2}$), are not of a large enough magnitude completely to obscure broad-line regions and, hence, to explain the narrow-line classification.

Since Mrk 205 has been presented in an earlier paper, its spectrum has not been re-fitted. However, from Reeves *et al.* (2001), we find that the spectral slope for Mrk 205 is 1.80 ± 0.04 , for the energy band 2.5–10 keV. This includes two Gaussian components: a narrow ($\sigma = 10$ eV) line at $E = 6.39 \pm 0.02$ keV and a broader ($\sigma = 250^{+190}_{-130}$ eV) one at $E = 6.74 \pm 0.12$ keV. The broad-band spectrum shows a slight soft excess, and is best fitted by $\Gamma = 1.86 \pm 0.02$ and a blackbody component with $kT = 120 \pm 8$ eV, together with the two emission lines. It is clear that these values for the slopes are consistent with those for the objects presented in this paper.

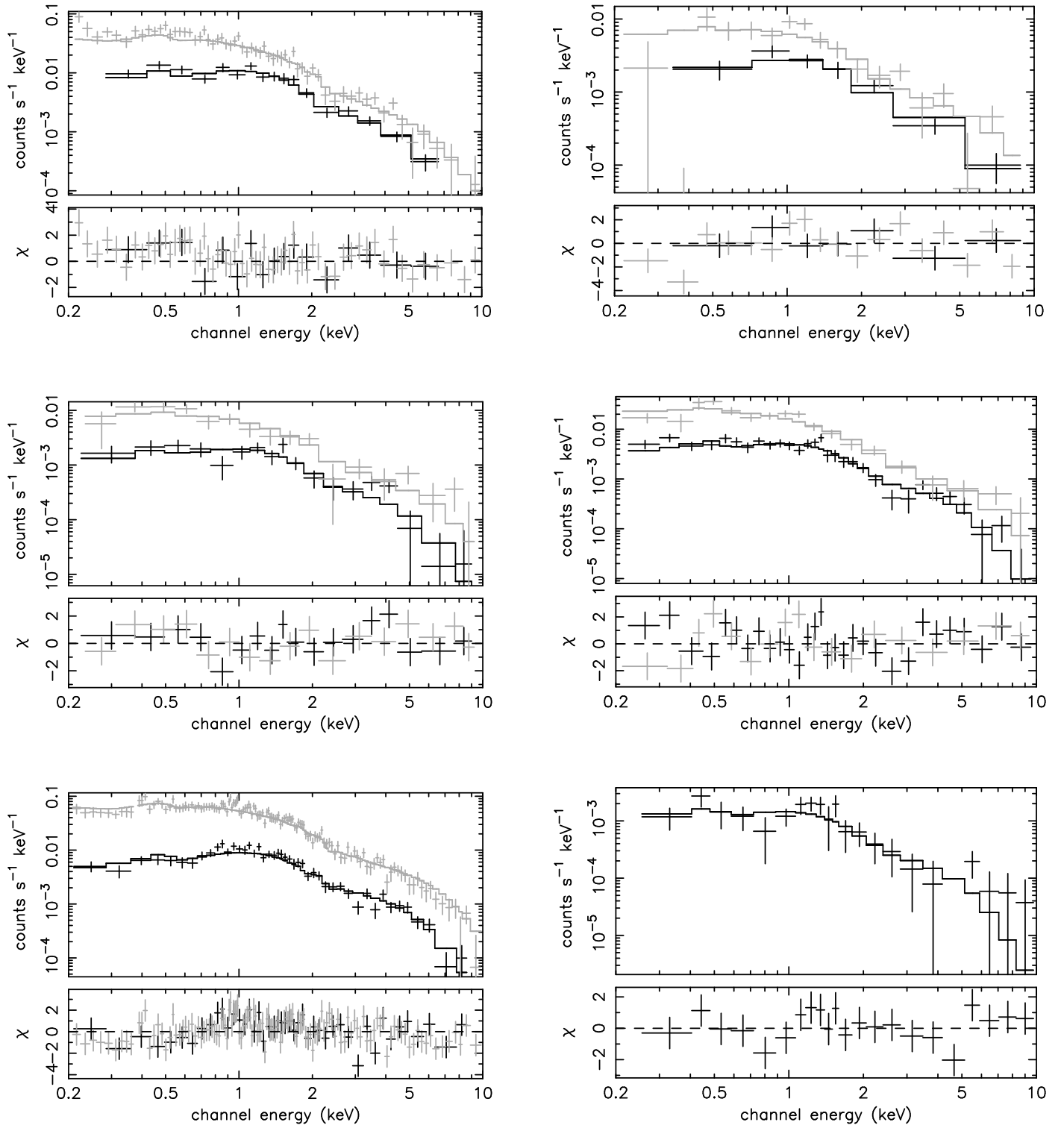


Figure 4. Broad band spectra for those QSOs with a 2–10 keV flux of greater than 5×10^{-14} erg cm $^{-2}$ s $^{-1}$. From top to bottom, the objects are XMMU J122052.0+750529, XMMU J122135.5+750914, XMMU J122206.4+752613 in the left-hand column; XMMU J122258.1+751934, XMMU J122351.0+752227 and XMMU J013233.2-395445 on the right.

Table 2. Power law slopes over a range of energy bands for the sources in the combined Mrk 205 and QSO 0130–403 fields.

Source ID	z	2–10 keV rest frame Γ	0.5–3 keV rest frame Γ	3+ keV rest frame Γ	0.2–10 keV obs. frame Γ
XMMU J121819.4+751919	2.649	2.05 ± 0.41	3.36 ± 0.72	2.44 ± 0.45	2.29 ± 0.18
XMMU J122048.4+751804	1.687	1.95 ± 0.36	2.21 ± 0.38	1.54 ± 0.32	1.66 ± 0.15
XMMU J122051.7+752820	0.181	1.64 ± 1.37	2.37 ± 0.39	4.28 ± 3.04	1.94 ± 0.25
XMMU J122052.0+750529	0.646	1.68 ± 0.10	1.83 ± 0.07	1.74 ± 0.15	1.77 ± 0.04
XMMU J122111.2+751117	1.259	2.13 ± 0.30	2.08 ± 0.16	1.30 ± 0.33	2.18 ± 0.10
XMMU J122120.5+751616	0.340	1.82 ± 0.44	2.34 ± 0.18	1.93 ± 1.04	2.19 ± 0.12
XMMU J122135.5+750914	0.330	1.26 ± 0.26	1.91 ± 0.17	1.48 ± 0.50	1.69 ± 0.10
XMMU J122206.4+752613	0.238	1.77 ± 0.07	1.50 ± 0.04	1.72 ± 0.13	1.56 ± 0.02
XMMU J122242.6+751434	1.065	2.61 ± 0.36	2.19 ± 0.81	-0.73 ± 2.05	2.40 ± 0.52
XMMU J122258.1+751934	0.257	1.74 ± 0.29	1.46 ± 0.18	2.00 ± 0.61	1.41 ± 0.09
XMMU J122318.5+751504	1.509	1.43 ± 0.29	2.41 ± 0.30	2.30 ± 0.49	2.05 ± 0.15
XMMU J122344.7+751922	0.757	1.74 ± 0.59	2.67 ± 0.17	2.24 ± 0.98	2.63 ± 0.13
XMMU J122351.0+752227	0.565	1.72 ± 0.17	1.94 ± 0.09	1.39 ± 0.26	1.88 ± 0.05
XMMU J122445.5+752224	1.852	2.17 ± 0.36	1.26 ± 0.44	2.08 ± 0.43	1.87 ± 0.16
XMMU J013302.0–400628	3.023	2.10 ± 0.07	2.08 ± 0.10	1.90 ± 0.06	1.89 ± 0.03
XMMU J013257.8–401030	2.180	1.67 ± 0.23	2.56 ± 0.25	1.91 ± 0.25	1.94 ± 0.10
XMMU J013314.7–401212	1.49	2.27 ± 0.58	2.42 ± 0.27	1.53 ± 0.47	2.65 ± 0.17
XMMU J013205.4–400047	2.12	2.05 ± 0.16	2.55 ± 0.16	2.21 ± 0.22	2.31 ± 0.08
XMMU J013348.3–400233	2.11	3.48 ± 1.14	1.22 ± 1.03	1.47 ± 1.14	2.33 ± 0.41
XMMU J013233.2–395445	1.73	1.77 ± 0.38	2.20 ± 0.57	2.54 ± 0.54	1.76 ± 0.19
XMMU J013333.8–395554	1.90	2.21 ± 0.32	2.47 ± 0.34	2.59 ± 0.49	2.19 ± 0.15
XMMU J013408.6–400547	2.14	2.33 ± 0.25	2.64 ± 0.17	2.10 ± 0.33	2.59 ± 0.10
XMMU J013320.4–402021	2.25	1.37 ± 0.61	1.10 ± 1.57	1.49 ± 0.60	1.33 ± 0.31
Mean		1.88 ± 0.04	2.07 ± 0.04	1.87 ± 0.05	1.76 ± 0.01

5 DISCUSSION

5.1 Absorbing Column Density

Our fits to the QSO spectra implied that the RQQs observed have no additional absorption above that due to our own Galaxy. The flatter spectral slopes for some objects could not be explained by obscuration in the AGN; this agrees with the *XMM* observation of the Lockman Hole (Hasinger *et al.* 2001; Mainieri *et al.* 2002), in that our sources are type-1 AGN, while their intrinsically absorbed objects are mainly type-2. One possibility is that we are not reaching a low enough ($< 10^{-14}$ erg cm $^{-2}$ s $^{-1}$) flux level to be measuring spectra of these faint, obscured sources, within these two fields.

However, the lack of any absorption above the Galactic value agrees with previous studies of radio-quiet QSOs, e.g., with *Einstein* (Canizares & White 1989; objects with $0.1 < z < 3.5$), *ROSAT* (Yuan *et al.* 1998; $z > 2$) and *Ginga* (Lawson & Turner 1997; $z < 1.4$). Indeed the radio-quiet QSOs in this sample appear to remain unabsorbed up to redshifts of $z \sim 3$.

Radio-loud objects, on the other hand, do tend to show excess absorption (e.g., Elvis *et al.* 1994; Brinkmann, Yuan & Siebert 1997; RT00). The data from RT00 show an average column density of 1.29×10^{22} cm $^{-2}$ for radio-loud quasars. For the sample of RQQs in this paper, a mean of 2.96×10^{21} cm $^{-2}$ is found for the *upper limits*, which is noticeably smaller.

It is known that the low-energy response of the *ASCA* SIS has been degrading over time (see Yaqoob *et al.* 2000). The effect of this is an underestimate of the soft X-ray

flux, which can show itself as an increase in N_H . In order to check that the differences found between the RLQ and RQQ distributions are not instrument-linked, the measured column densities for two objects which have been observed by both *XMM* and *ASCA* were compared (*ASCA* values were taken from RT00; *XMM* values calculated for our own data for PKS 0558–504 and taken from Reeves *et al.* 2001 for Mrk 205). It was found that, within the errors, the instruments agreed; it can, therefore, be assumed that the absorption measured for the RT00 radio-loud sample is not due simply to the *ASCA* calibration.

Statistical tests were applied to both the radio-quiet objects from this paper and the radio-loud ones from RT00, to determine whether there was evidence for a difference in population. Fig. 5 shows the column densities against redshift for this combined sample, with the *ASCA*-detected RLQs marked by crosses and the *XMM* RQQs by circles/arrows.

Due to the overwhelming presence of censored data (that is, upper limit measurements), the *ASURV* (Astronomy Survival Analysis) software was used (see Feigelson & Nelson 1985). Employing each of the possible two-sample tests, we found that the probability that the RQQs and RLQs are from the same population was very low: < 0.01 per cent. The Kolmogorov–Smirnov test was also performed on the data, leading to a probability of ~ 3.4 per cent for the existence of one population only. Other statistical tests were also tried, each method confirming the same result: the radio-quiet QSOs in our sample were found to belong to a different population from the radio-loud objects in RT00 (probability of > 99.99 per cent in general).

Summarising, we find that, although RLQs tend to show

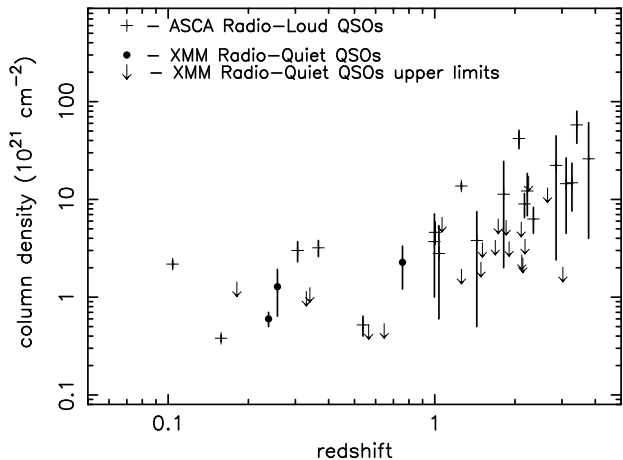


Figure 5. The joint sample of radio-quiet and radio-loud QSOs, from *XMM* and *ASCA* (taken from Reeves & Turner 2000) respectively.

excess absorption at high redshifts, RQQs do not, at least up to $z \sim 3$. This implies that there is an intrinsic difference in the local environment of the two types of QSO at high redshifts. It must be noted that the situation for radio-quiet QSOs at higher redshifts ($z > 5$) is unclear; deep *XMM* observations of individual, bright high-redshift QSOs are required to explore this possibility.

5.2 Spectral Evolution

The QSOs in this sample all show the same range of continuum photon indices, regardless of luminosity or redshift, over the energy range 2–10 keV. Comparing the slopes over the full 0.2–10 keV range gave the same results.

Canizares & White (1989) also find no evidence for a Γ - z dependence from the *Einstein* data, up to a maximum energy of 4 keV. Likewise, Yuan *et al.* (1998) found that the spectral slopes of distant ($z > 2.5$) RQQs were consistent (within the errors) with those of nearby objects; *ROSAT* covered the energy range 0.1–2.4 keV. The *ASCA* data in RT00 also showed no significant correlation between Γ and redshift, over a similar energy range to that of *XMM*. The independence of spectral slope and redshift is also observed in the higher energy band ($E \geq 2$ keV) of radio-loud objects [e.g., comparison between Γ from *EXOSAT* data (Lawson *et al.* 1992) and *Ginga* (Williams *et al.* 1992)]. There also appears to be no evolution with redshift of the extreme-ultraviolet spectral slope, for either RL or RQQs (Telfer *et al.* 2002).

The link between the different regions of the spectral energy distributions of AGN is, as yet, uncertain, with no complete theory having been generally accepted. The observed lack of correlation between slope and redshift may suggest, however, that the luminosity of these QSOs is simply scaling as the black hole mass – i.e. \dot{M} remains constant with respect to the Eddington value, as the overall spectral energy distribution remains unchanged. Different values of the accretion rate could then be responsible for some of the dispersion of the spectral slopes that is observed (e.g., Liu, Mineshige & Shibata 2002). Alternatively, the spread of Γ may be due to different disc-corona geometries (Czerny &

Elvis 1987; Fabian *et al.* 2002). It should be noted that this dispersion in slope is also observed in the low-luminosity Seyferts, as well as QSOs: Narrow Line Seyfert 1 galaxies tend to have softer spectra than the corresponding broader line objects; this may be explained if these objects are accreting at a greater fraction of the Eddington rate, when compared to the broad line AGN (Pounds, Done & Osborne 1995).

5.3 Spectral Curvature

For the signal-to-noise of the data presented here, it is not possible to make a conclusive statement on the presence or absence of reflection in the *individual* QSOs in this sample. However, the spectral hardening (where $\Delta\Gamma = 0.2$) that appears to exist for the sample as a whole above 3 keV, is consistent with reflection from 2π steradians of optically thick matter, located out of the line of sight.

Past studies (e.g., with *ASCA*, RT00) have noted that the strength of the neutral Compton reflection hump, and the associated iron $K\alpha$ line, is considerably lower in the higher-redshift QSOs, than that expected in Seyfert 1 galaxies at low redshift (e.g., Nandra & Pounds 1994). However, the QSO spectra previously obtained above $z = 2$ by *ASCA* were dominated by core-dominated radio-loud quasars, where a contribution from the relativistic jet could weaken any apparent reflection features. This does not appear to be the case for the *radio-quiet* AGN found in this sample; the average co-added spectra of these AGN above $z = 2$ appears to indicate the presence of a reflection component with $R \sim 1$, the first time this has been observed for high-redshift QSOs. Such a reflection component could naturally arise from X-rays scattering off optically thick material, such as the inner accretion disc, subtending $\sim 2\pi$ steradians to the X-ray source. Another possible contribution is by reflection off a distant molecular torus, predicted from AGN unification schemes. We note here that such a component may account for the ‘narrow’ iron $K\alpha$ lines observed by *XMM-Newton* and *Chandra* in bright, nearby AGN (e.g., Kaspi *et al.* 2001; O’Brien *et al.* 2001a).

Finally we note the possibility that the reflection may occur from an ionised disc (e.g., Reeves *et al.* 1997; Eracleous & Halpern 1998; Grandi *et al.* 2001; Ballantyne, Ross & Fabian 2002). However, the data in this paper show only one significant iron line, located near 6.6 keV; this tentatively suggests that the reprocessing material might be more strongly ionised in some of the higher luminosity AGN, as is observed for instance in the *XMM-Newton* spectrum of Mrk 205 (Reeves *et al.* 2001). Such an ionised disc could also explain some of the observed spectral curvature (e.g., O’Brien *et al.* 2001b; Pounds *et al.* 2001).

6 CONCLUSIONS

Analysing 23 radio-quiet QSOs, with a mean redshift of 1.40 and 2–10 keV luminosity of 9.66×10^{44} erg s^{-1} , we have found the following:

- The 2–10 keV spectral slopes measured for this sample show a significant scatter. However there is no obvious trend with redshift, so it can be concluded that there is no

evidence for X-ray spectral evolution of QSOs with redshift or luminosity

- The mean value for α_{ox} is measured to be -1.66 ± 0.04 . Within the sample there is no correlation with redshift, although comparison with both lower and higher redshift samples indicates a slight steepening as z increases.
- The dispersion in photon index is intrinsic; that is, it is not related to obscuration, as is thought to be the case for the faint sources constituting X-ray background.
- No excess absorption in the rest frame of the radio-quiet QSOs is found. This is in contrast to the additional N_H measured by past studies in high- z radio-loud quasars and suggests an intrinsic difference could exist in the local environments of the two classes of QSO.
- Considering the sample as a whole, the spectral slope appears to flatten at higher energies (above 3 keV). This indicates the presence of a reflection component from material subtending a solid angle of 2π steradians to the X-ray source. This matter could arise from either the inner accretion disc or a distant (>1 pc) molecular torus.

7 ACKNOWLEDGMENTS

The work in this paper is based on observations with *XMM-Newton*, an ESA science mission, with instruments and contributions directly funded by ESA and NASA. The authors would like to thank the EPIC Consortium for all their work during the calibration phase, and the SOC and SSC teams for making the observation and analysis possible. Thanks also go to Xavier Barcons and the AXIS team for the data on the QSOs in the field of Mrk 205, together with the anonymous referee, for very helpful comments. This research has made use of the NASA/IPAC Extragalactic Database (NED), which is operated by the Jet Propulsion Laboratory, California Institute of Technology, under contract with the National Aeronautics and Space Administration. For the survival statistics, the *ASURV* v1.1 (Astronomy Survival Analysis) software was utilised (Feigelson & Nelson 1985). Support from a PPARC studentship and the Leverhulme Trust is acknowledged by KLP and JNR respectively.

REFERENCES

- Adam G., 1985, *A&AS*, 61, 225
 Antonucci R., 1993, *ARA&A*, 31, 473
 Ballantyne D.R., Ross R.R., Fabian A.C., 2002, *MNRAS*, 332, L45
 Barcons X. *et al.*, 2002, *A&A*, 382, 522 (XB02)
 Bechtold J. *et al.*, 1994, *AJ*, 108, 759
 Brinkmann W., Yuan W., Siebert J., 1997, *A&A*, 319, 413
 Canizares C.R., White J.L., 1989, *ApJ*, 339, 27
 Czerny B., Elvis M., 1987, *ApJ*, 321, 305
 Dickey J.M., Lockman F.J., 1990, *ARA&A*, 28, 251
 Elvis M., Fiore F., Wilkes B., McDowell J., Bechtold J., 1994, *ApJ*, 422, 60
 Eracleous M., Halpern J.P., 1998, *ApJ*, 505, 577
 Fabian A.C., Ballantyne D.R., Merloni A., Vaughan S., Iwasawa K., Boller Th., 2002, *MNRAS*, 331, L35
 Falomo R., Kotilainen J., Treves A., 2001, *ApJ*, 547, 124
 Feigelson E.D., Nelson P.I., 1985, *ApJ*, 293, 192
 Grandi P., Maraschi L., Urry C.M., Matt G., 2001, *ApJ*, 556, 35
 Hasinger G. *et al.*, 2001, *A&A*, 365, L45
 Kaspi S. *et al.*, 2001, *ApJ*, 554, 216
 Kellerman K.I., Sramek R., Schmidt M., Shaffer D.B., Green R., 1989, *AJ*, 98, 1995
 Kukula M.J., Dunlop J.S., Hughes D.H., Rawlings S., 1998, *MNRAS*, 297, 366
 Lamer G., Brunner H., Staubert R., 1997, *A&A*, 327, 467
 Lawson A.J., Turner M.J.L., Williams O.R., Stewart G.C., Saxton R.D., 1992, *MNRAS*, 259, 743
 Lawson A.J., Turner M.J.L., 1997, *MNRAS*, 288, 920
 Liu B.F., Mineshige S., Shibata K., 2002, *ApJ*, 572, L173
 Maccacaro T., Gioia I.M., Wolter A., Zamorani G., Stocke J.T., 1988, *ApJ*, 326, 680
 Magdziarz P., Zdziarski A.A., 1995, *MNRAS*, 273, 837
 Mainieri V., Bergeron J., Hasinger G., Lehmann I., Rosati P., Schmidt M., Szokoly G., Della Ceca R., 2002, *A&A*, in press (astro-ph/0207166)
 Miller L., Peacock J.A., Mead A.R.G., 1990, *MNRAS*, 244, 207
 Nandra K., Pounds K.A., 1994, *MNRAS*, 268, 405
 O'Brien P.T., Page K., Reeves J.N., Pounds K., Turner M.J.L., Puchnarewicz E.M., 2001a, *MNRAS*, 327, L37
 O'Brien P.T., Reeves J.N., Turner M.J.L., Pounds K.A., Page M., Gliozzi M., Brinkmann W., Stephen J.B., Dadina M., 2001b, *A&A*, 365, L122
 Pounds K.A., Nandra K., Stewart G.C., George I.M., Fabian A.C., 1990, *Nat*, 344, 132
 Pounds K.A., Done C., Osborne J., 1995, *MNRAS*, 277, L5
 Pounds K., Reeves J., O'Brien P., Page K., Turner M., Nayakshin S., 2001, *ApJ*, 559, 181
 Pounds K.A., Reeves J.N., 2002, in *New Visions of the X-ray Universe in the XMM-Newton and Chandra era* (astro-ph/0201436)
 Reeves J.N., Turner M.J.L., Ohashi T., Kii T., 1997, *MNRAS*, 292, 468
 Reeves J.N., Turner M.J.L., 2000, *MNRAS*, 316, 234 (RT00)
 Reeves J.N., Turner M.J.L., Pounds K.A., O'Brien P.T., Boller Th., Ferrando P., Kendziorra E., Vercellone S., 2001, *A&A*, 365, 134
 Smith M.G., 1976, *ApJ Letters*, 206, L125
 Strüder L. *et al.*, 2001, *A&A*, 365, L18
 Telfer R.C., Zheng W., Kriss G.A., Davidsen A.F., 2002, *ApJ*, 565, 773
 Turner M.J.L. *et al.*, 2001, *A&A*, 365, L27
 Véron-Cetty M.-P., Woltjer L., 1990, *A&A*, 236, 69
 Véron-Cetty M.-P., Véron P., 2001, *A&A*, 374, 92
 Vignali C., Brandt W.N., Fan X., Gunn J.E., Kaspi S., Schneider D.P., Strauss M.A., 2001, *AJ*, 122, 2143
 Wilkes B.J., Elvis M., 1987, *ApJ* 323, 243
 Williams O.R. *et al.*, 1992, *ApJ*, 389, 157
 Worrall D.M., Giommi P., Tananbaum H., Zamorani G., 1987, *ApJ*, 313, 596
 Yaqoob T. *et al.*, 2000, *ASCA Guest Observer Facility Calibration Memo*, ASCA-CAL-00-06-01 (<http://asca.gsfc.nasa.gov/docs/asca/calibration/nhparam.html>)
 Yuan W., Brinkman W., Siebert J., Voges W., 1998, *A&A*, 330, 108
 Zamorani G. *et al.*, 1981, *ApJ*, 245, 357